

Improvement in Corrosion Behavior of Al–Ti Alloy by Adding 2 wt% Magnesia and 1 wt% Silicon Carbide

Rana Afif Anae¹ · Wafaa Mahdi Salih¹ · Ban Farhan Dawood¹

Received: 11 September 2016/Revised: 8 May 2017/Accepted: 3 July 2017/Published online: 10 July 2017
© Springer International Publishing AG 2017

Abstract Aluminum building wire wastes were used to produce Al alloy by adding 4 wt% of titanium. Also, aluminum matrix composite was fabricated by adding 2 wt% MgO–1 wt% SiC to investigate the corrosion behavior of Al–Ti alloy and composite before and after heat treatments. The heat treatments included annealing, normalizing and tempering at 500 °C. The heat treatments led to breaking up the main phase in base alloy (Al₃Ti) and occur many reactions involve decomposition of SiC to form Al₄C₃ and reaction of MgO to form spinel MgO·Al₂O₃. The fabricated alloy and composite were characterized by XRD, SEM and EDS. Optical microscopy was used to investigate the changes after heat treatments. Corrosion measurement was achieved in seawater by potentiostat at scan rate of 5 mV s⁻¹. Corrosion parameters were measured for base alloy and composite by Tafel extrapolation method. Corrosion potentials were varied after heat treatments due to variation in anodic and cathodic sites on surface, while the corrosion current densities of composite were less than for base alloy due to the role of SiC and MgO particles that led to reduce the anodic sites on metallic surface. Cyclic polarization test showed that the fabricated composite had breakdown potential more positive than for fabricated alloy.

Keywords AMC · Al–Ti alloy · SiC particles · MgO particles · Corrosion · Heat treatment

1 Introduction

Metal matrix composites take a wide range of applications in many industries, especially with aluminum matrix composites. The authors tried to add different types of reinforcements such as alumina, zirconia, magnesia, graphite, carbides and other compounds to improve the properties of these composites. Corrosion behavior of composites shows different trends of material due to the role of the added reinforcement and how it can be incorporated into matrix. Many authors focus on the corrosion behavior of composites in different media. Jamaludin et al. [1] studied the effect of alumina and silicon carbide on corrosion behavior of Al–Cu–Mg alloy, Bobic et al. [2] showed the role of different reinforcements on the corrosion behavior of Al matrix composite, El-Sayed et al. [3] investigated the effects of graphite on the corrosion behavior of aluminum–graphite composite, Ahmed et al. [4] studied the effect of copper and silicon carbide content on the corrosion resistance of Al–Mg Alloys, also Muthazhagan et al. [5] studied corrosion behavior of aluminum–boron carbide–graphite composites, Rana et al. [6] investigated the effect of SiO₂ particles on corrosion of Al–Cu–Mg, in another research, Rana studied the corrosion behavior of Al–Si–Cu/Y₂O₃ [7] and Al–Si–Cu/WC [8] in basic medium, and Muna et al. [9] studied the corrosion behavior of 6061/SiC composites in seawater.

The aim of present work is recycling of Al building wires to produce Al alloy and improving this alloy by adding Ti and ceramic particles including 2 wt% MgO and 1 wt% SiC as reinforcement for Al–Ti alloy. Corrosion behavior of produced alloy and composite was investigated in seawater before and after heat treatments at 500 °C.

✉ Rana Afif Anae
Dr.rana_afif@yahoo.com

¹ Department of Materials Engineering, University of Technology, Baghdad, Iraq

2 Experimental Procedure

2.1 Preparation of Specimens

Al building wire wastes were used to produce Al alloy. 4 wt% of Ti was added to fabricate Al–Ti alloy with particle size 165 μm , while 1 wt% of each MgO and SiC particle was added to fabricate Al–Ti matrix composite with 53 and 20 μm of MgO and SiC, respectively. For the production of composite specimen, matrix material Al was put in the crucible and the melting process was started and continued until the temperature of the liquid matrix reached 700 °C. Stirring apparatus was immersed in the liquid metal, and then, appropriate amount of Ti and then MgO and SiC were added in the liquid metal by a funnel during the stirring process. After the addition of reinforcements to liquid matrix, the mixture was stirred for about 7 min at 500 rpm in order to allow homogeneous distribution of MgO and SiC particles in the mixture. When stirring was completed, the liquid melt was poured into steel mold of 20 mm diameter and 170 mm height and was allowed to cool down at room temperature.

The specimens of alloy and composite were cut as cylindrical shapes for characterization and corrosion test with dimensions of 20 mm diameter and 4 mm length. Grinding and polishing were performed with emery papers of 220, 400, 500, 800 and 1000 mesh grit and then rinsed with acetone.

2.2 XRF Analysis

X-ray fluorescence technique was performed to investigate the analysis of base alloy Al–Ti using XRF device (type A003 OLYMPUS). The chemical composition of fabricated alloy is listed in Table 1.

2.3 XRD Analysis

XRD was carried out by X-ray diffractometer, Model: XRD-6000 with Cu as target at voltage = 40.0 (kV) and current = 30.0 (mA).

2.4 SEM and EDS

The fabricated specimens were tested by scanning electron microscope and energy-dispersive spectroscopy using device-type VEGA3 TESCAN.

2.5 Heat Treatment

The specimens were subjected to annealing, normalizing and tempering processes. During annealing, the specimen was heated to 500 °C, held for 1 h, and allowed to cool in the furnace. For normalizing, the specimen was heated to 500 °C, held for 1 h, and allowed to cool in air. The tempering process was achieved by heating the specimen up to 500 °C, held for 1 h, then quenched rapidly in water, reheated to 100 °C, held at this temperature for 1 h, and then allowed to cool in air.

2.6 Optical Microscopy

The microstructure evolution was investigated by means of optical microscope using (BEL photonics) microscope that was connected to computer. The specimens were etched by Killers solution (2 ml HF + 3 ml HCl + 5 ml HNO₃ + 190 ml H₂O) as etchant for 10–30 s. for optical examination.

2.7 Corrosion

Corrosion test was achieved by a potentiostat with SCI electrochemical software at a scan rate of 5 mV s⁻¹. The voltages were applied when the rate at which open-circuit potential (E_{oc}) changed ± 200 mV. The main results obtained were expressed in terms of the corrosion potentials (E_{corr}) and corrosion current density (i_{corr}) by Tafel extrapolation method. All corrosion tests were carried out in artificial seawater (3.5 wt% NaCl solution).

3 Results and Discussion

3.1 Characterization

XRD analysis of fabricated Al–Ti alloy and Al–Ti/2% MgO–1% SiC composite is presented in Fig. 1. The most intensive peaks in the XRD spectrum for the Al matrix were in good agreement with JCPDS card (04-0787). The peaks of Al were overlapped with the peak of Al₃Ti phase according to JCPDS card (37-1449). In composite, the peaks of MgO and SiC also overlapped with the peaks of matrix according to JCPDS cards (30-0794) and (39-1196), respectively. The three strongest peaks in XRD analysis of alloy and composite are listed in Table 2.

Table 1 Chemical composition of base alloy

Metal	Ti	Si	P	Cu	S	Fe	Zn	Pb	Zr	Al
wt%	4.1	1.50	1.45	1.00	0.90	0.80	0.10	0.10	0.06	89.99

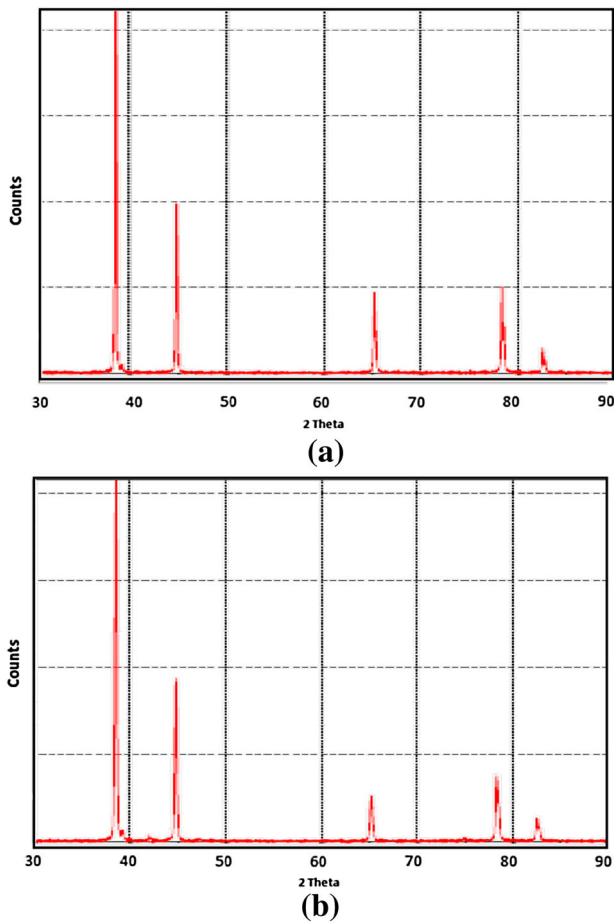


Fig. 1 XRD pattern of Al–Ti alloy (a) and Al–Ti composite reinforced with MgO and SiC (b)

Table 2 Strongest three peaks in XRD data for fabricated alloy and composite

Material	2θ (°)	Intensity	hkl
Alloy	38.5709	100	111
	44.8228	48	200
	78.3197	27	311
Composite	38.9748	100	111
	45.2025	80	012
	78.6401	53	021

The SEM and EDS inspections are shown in Figs. 2 and 3, respectively. In Fig. 2, the difference in color is an indicator for matrix, reinforcements and formed phases. SEM image of base alloy indicates the main phase (Al₃Ti), which appears in light gray compared with Al matrix with dark gray, while in SEM image of composite, the MgO particles appear as arms shape and segregate out of grain boundaries with light gray color in addition to show the clustering and non-homogeneous distribution of SiC particles in Al matrix (black color). This was due to the

variation of contact time between SiC particles and molten Al during casting process. Some places in Al matrix can be identified without SiC reinforcing particles. Porosities were observed in microstructure because when SiC particles were added to melted liquid during casting, they introduced air in the melt which entrapped between the particles [10].

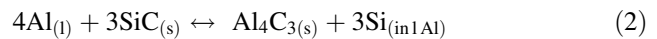
The EDS analysis in Fig. 3 shows the elements that contain in each fabricated alloy and composite. In the base alloy, can be seen Al and Ti only, while in composite can be seen the Al, Ti and the elements of reinforcements (Mg, Si, C and O).

Annealing, normalizing and tempering were achieved for both alloy and composite to investigate the role of ceramic reinforcement on microstructure and corrosion behavior of each material after heat treatment. Optical examination of structure before and after heat treatments indicates the presence Al₃Ti phase and uniformly distribution of MgO and SiC particles in Al matrix as shown in Fig. 4.

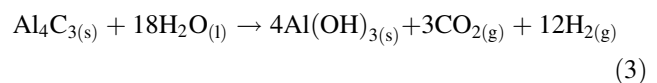
In binary Al–Ti alloys, Al₃Ti intermetallic particles disperse as Petal-like particles in α-Al solid solution according to following reaction:



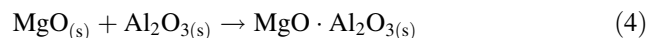
Al₃Ti crystals act as nuclei for grains to grow. Multiple nucleations of averagely eight sites may occur on each particle. In the presence of SiC in composite, the liquid aluminum tends to attack SiC according to the following reaction:



The Al₄C₃ compound has deleterious effects within the composite because, firstly, it is a brittle phase which degrades the mechanical properties, and secondly, it reacts with liquid water or with moisture in the ambient according to the following reaction:



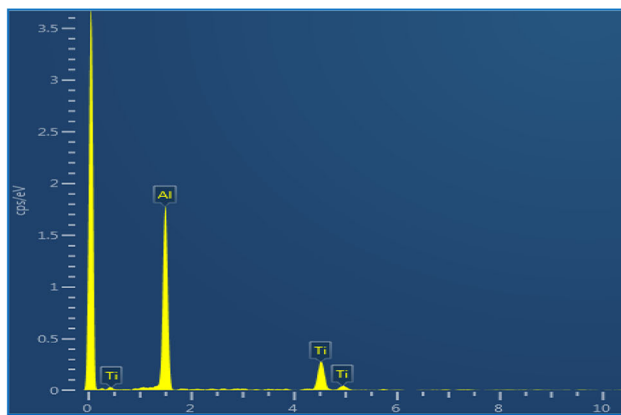
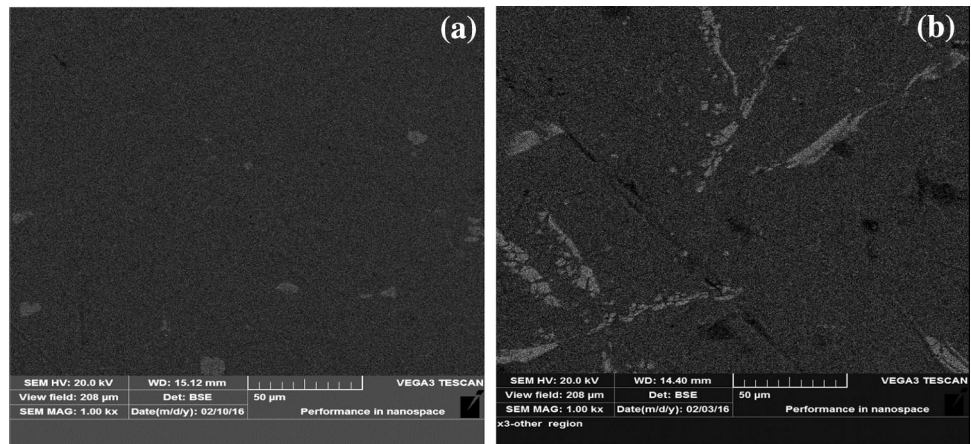
During the casting, some aluminum may convert to Al₂O₃. At the same time, the aluminum content oxidizes and then reacts with MgO to form a non-stoichiometric spinel as follows:



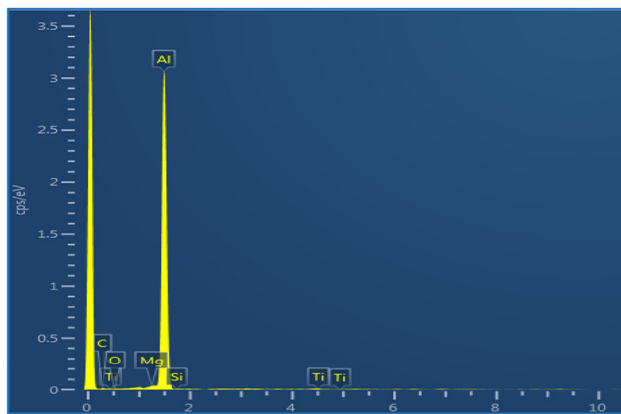
Some SiC particles in the composite might oxidize during heating, and then, SiO₂ film forms around the particle surface [11]. After that, 2MgO·SiO₂ forms at the boundaries between MgO and SiC particles, and its amount increases in the matrix with heating temperature and time.

The molten base alloy damages the integrity of MgO–SiC composites under high temperature. SiC particles can be directly dissolved into molten alloy. The interspaces that remain after SiC decomposition act as the route for Al–Ti penetration. MgO particles become isolated and dissolve

Fig. 2 SEM of Al–Ti alloy (a) and composite with MgO and SiC (b)



(a)



(b)

Fig. 3 EDS of Al–Ti alloy and composite with MgO and SiC

into the molten alloy. Also, the brittle reactant Al_4C_3 forms agglomerates at the interface leading to degradation of the composite strength, modulus and corrosion [12, 13].

3.2 Corrosion Measurement

Tafel plots of Al–Ti alloy and Al–Ti/2% MgO–1% SiC composite are shown in Fig. 5 for untreated and heat

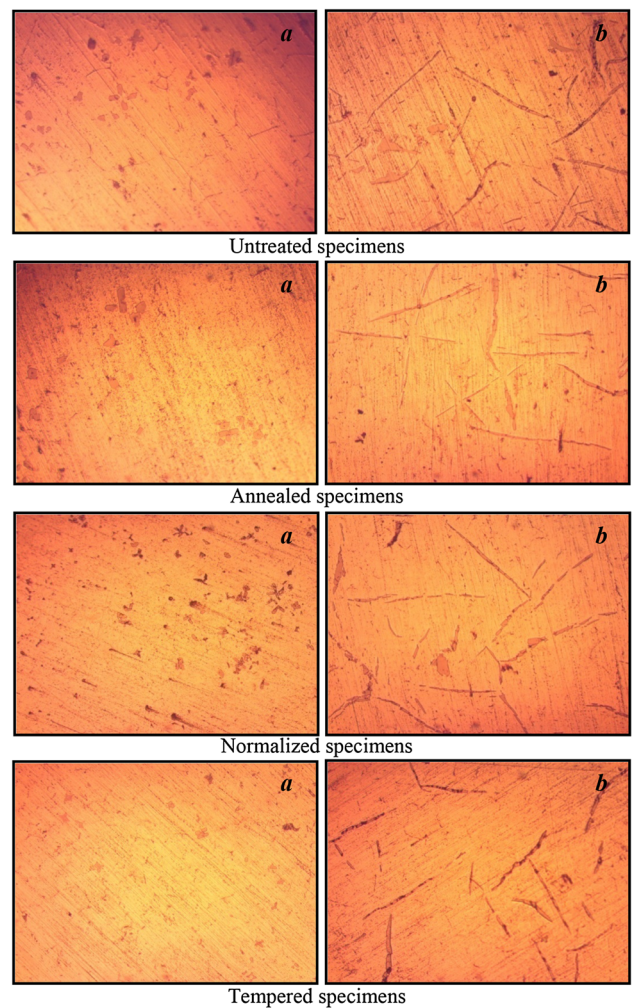


Fig. 4 Optical microscopies of base alloy (a) and composite (b)

treated specimens in 3.5% NaCl solution at room temperature. Aluminum alloys and composites undergo the corrosion in neutral medium according to the following reactions:

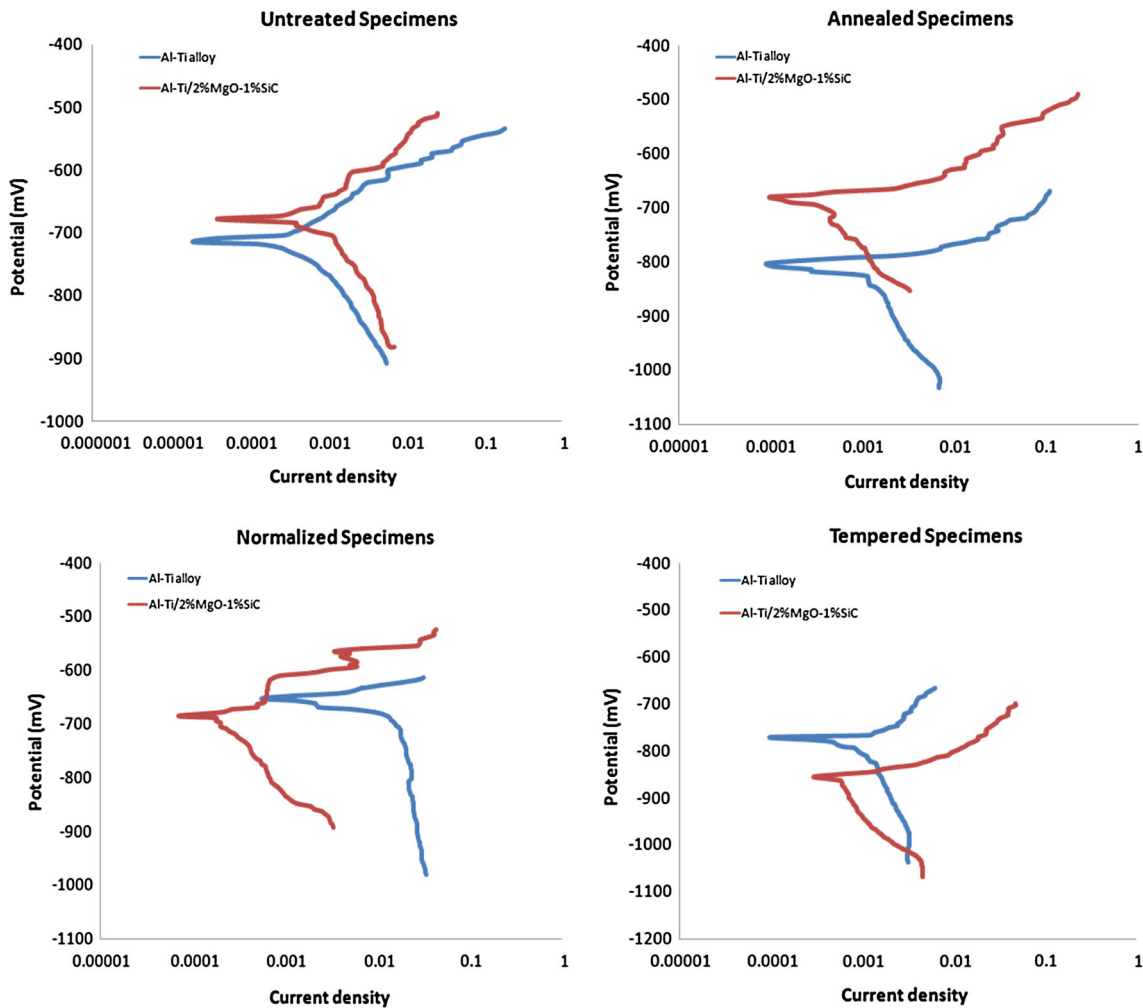
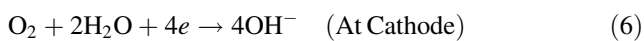
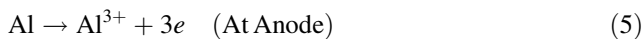


Fig. 5 Tafel plots of base alloy and composite before and after heat treatments



Generally, in the presence of chloride ions, the dissolution of metals enhances because of chloride ion which bonds chemically in the interface as an initial step of the formation of different mixed oxohydroxo-chloro complexes to produce finally the $[AlCl_6]^{3-}$ complex [14].

The corrosion potentials (E_{corr}) of composite were more noble than base alloy for untreated and annealed specimens, while they were less noble for normalized and tempered specimens. This means that the potential of the galvanic cell becomes more positive or negative, and hence, the Gibbs free energy change (ΔG) for the corrosion process becomes more negative or positive, respectively. The corrosion reaction is then expected to be more or less spontaneous on pure thermodynamic ground and vice versa. It is thus shown that (E_{corr}) value is a measure for the extent of the feasibility of the corrosion reaction on purely thermodynamic basis, while, in general, the corrosion

current densities (i_{corr}) of composite were less than for alloy before and after heat treatments. It is known that any factor that enhances the value of (i_{corr}) enhances the value of the corrosion rate on pure kinetic ground.

The rate (C_R mpy) of corrosion in a given environment is directly proportional to its corrosion current density (i_{corr}) in accordance with the relation [15, 16]:

$$C_{R(\text{mpy})} = 0.13 \times i_{\text{corr}} \times \left(\frac{e}{\rho}\right) \quad (7)$$

where C_R (mpy) is corrosion rate in mil per year, e , equivalent weight of alloy (g), and ρ , density of alloy (g/cm^3).

The data of corrosion rate show, in general, that reinforcing the base alloy with MgO and SiC particles led to get less corrosion rate, i.e., less probability to dissolution of metals from material.

The Tafel slopes were influenced in the presence of reinforcements. Generally, the composite had Tafel slopes less than for alloy, and the heat treatments led to increasing

Table 3 Corrosion data of base alloy and composite in seawater

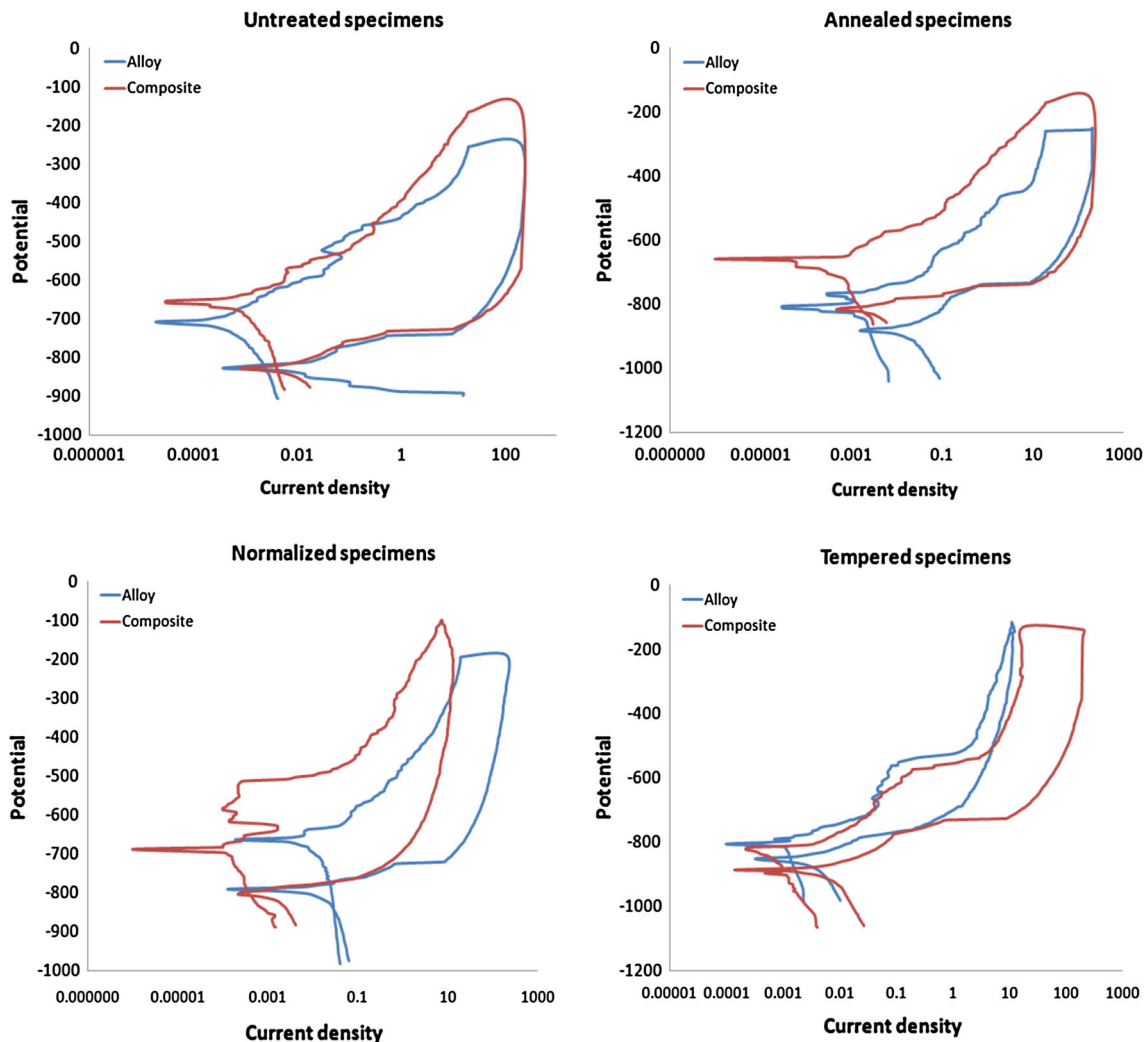
Material	Conditions	E_{corr} (mV)	I_{corr} ($\mu\text{A}/\text{cm}^2$)	$-b_c$ (mV/dec $^{-1}$)	$+b_a$ (mV/dec $^{-1}$)	$R_p \times 10^3$ ($\Omega \text{ cm}^2$)	C_R (Mpy)
Alloy	Untreated	-714	0.4142	77.3	85.4	42.53	0.178
Composite		-678	0.2905	60.8	74.6	50.07	0.126
Alloy	Annealed	-806	0.8077	175.3	34.5	15.50	0.350
Composite		-682	0.2946	171.2	27.8	35.25	0.128
Alloy	Normalized	-652	10.220	244.1	50.5	1.777	4.425
Composite		-684	0.1553	145.1	33.4	75.91	0.067
Alloy	Tempered	-771	0.6672	212.3	61.1	30.88	0.289
Composite		-854	0.5556	201.4	55.4	33.96	0.241

Tafel slopes for both fabricated materials. Also after heat treatments, the cathodic Tafel slope (b_c) became higher than anodic slope (b_a). It is inferred that the rate of change of current with change of potential was smaller during cathodic polarization than that during anodic polarization.

The small anodic slope (b_a) indicates that the presence of a film on the surface of the tested material is less

permeable and can even obstruct the metal dissolution reaction but still permits an electrochemical reaction to occur. It is known that the surface oxide on aluminum alloys permits the movement of ionic species and an electron or vacancy flux across it [17, 18].

The polarization resistance (R_p) may be defined as the slope of a potential–current density; the polarization

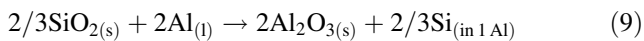
**Fig. 6** Cyclic polarization of base alloy and composite before and after heat treatments

resistance can be determined from the Tafel slopes, and according to Stern–Geary equation [19, 20]:

$$R_p = \left(\frac{dE}{di} \right)_{i=0} = \frac{b_c b_a}{2.303(b_c + b_a) i_{corr}} \quad (8)$$

Generally, the composite has polarization resistance more than base alloy as listed in Table 3.

The lowest corrosion rate (0.067 mpy) and highest polarization resistance ($75.9 \times 10^3 \Omega \text{ cm}^2$) were for normalized Al–Ti/MgO–SiC composite. Although breaking up the hard phase (Al_3Ti) and introducing the cracks by cooling in air for normalizing process, the presence of MgO and SiC together in composite gave resistance for base alloy due to the formation of $\text{MgO} \cdot \text{Al}_2\text{O}_3$ and $2\text{MgO} \cdot \text{SiO}_2$. Also, the chemical reaction between molten aluminum and SiO_2 is also thermodynamically possible [21] according to the following reaction:



This means that the heat treatment forms many oxides on Al composite surface such as Al_2O_3 , SiO_2 and maybe TiO_2 ; these oxides enhance the corrosion resistance of experimental composite.

3.3 Cyclic Polarization

Figure 6 shows the cyclic polarization for fabricated alloy and composite before and after heat treatments to measure pitting susceptibility for material. These curves indicate that the potentials for the reverse scan are less positive than those for the forward scan with breakdown potential for composite more positive than for alloy.

Generally, pits in the Al/SiC composites are deeper than those in the Al/ Al_2O_3 composites, probably because the SiC particles acted as efficient cathodic sites and because preferential attack occurs at the reinforcement/matrix interface. Furthermore, pores, matrix second phases and interfacial reaction products can all influence corrosion behavior of SiC/Al composite in a significant way. On the other hand, the high corrosion resistance of Al/SiC composite is in good agreement with other studies, where SiC does not substantially affect pitting attack on some aluminum alloys, and the pits were smaller and shallower than those on the unreinforced alloy [22]. In the tested composite, MgO and SiC affect together to reduce pitting corrosion in Al–Ti alloy.

4 Conclusion

Using Al wire wastes to fabricate Al–Ti alloy and then reinforcing this alloy by 2 wt% MgO and 1 wt% SiC by stir casting method has been achieved to investigate the

corrosion behavior of fabricated alloy and composite in seawater at room temperature.

By some inspections including XRD, SEM and EDS, the characterization was performed to show the reactions that occur between reinforcements and Al matrix, especially after heat treatments. Many oxides will be formed on surface, which lead to enhance the passive film of Al_2O_3 on Al alloy and composite surface. In present composite, MgO and SiC affected together to improve the corrosion behavior of fabricated materials.

References

- Jamaludin SB, Yusoff Z, Ahmad KR (2008) Comparative study of corrosion behavior of AA2014/15 Vol% Al_2O_3 and AA2009/20 Vol% SiC_w. *Port Electrochim Acta* 26:291–301
- Bobic B, Mitrovic S, Babic M, Bobic I (2010) Corrosion of metal–matrix composites with aluminium alloy substrate. *Tribol Ind* 32(1):3–11
- Sherif ESM, Almajid AA, Latif FH, Junaedi H (2011) Effects of graphite on the corrosion behavior of aluminium–graphite composite in sodium chloride solutions. *Int J Electrochem Sci* 6:1085–1099
- Mayyas AT, Hamasha MM, Alrashdan A, Hassan AM, Hayajneh MT (2012) Effect of copper and silicon carbide content on the corrosion resistance of Al–Mg alloys in acidic and alkaline solutions. *J Miner Mater Charact Eng* 11(4):435–452
- Muthazhagan C, Gnanavelbabu A, Rajkumar K, Bhaskar GB (2014) Corrosion behavior of aluminium–boron carbide–graphite composites. *Appl Mech Mater* 591:51–54
- Rana AM, Mervit M, Al-Kaisy HA, Abdul Maged SA (2014) Corrosion behavior for Al–Cu–Mg alloy by addition of SiO_2 particles in seawater. *Eng Technol J* 32, Part (A)(2):354–364
- Anaee RA (2014) Thermodynamic and kinetic study for corrosion of Al–Si–Cu/ Y_2O_3 composites. *Asian J Chem* 26(14):4469–4474
- Anaee RA (2015) Study of corrosion behavior of Al–Si–Cu/WC composites in 0.1 N NaOH solution. *J King Abdulaziz Univ Eng Sci* 26(1):55–65. doi:10.4197/Eng.26-1.3
- Abbass MK, Hassan KS, Alwan AS (2015) Study of corrosion resistance of aluminum alloy 6061/SiC composites in 3.5% NaCl solution. *Int J Mater Mech Manuf* 3(1):31–35
- Shorowordi KM, Laoui T, Haseeb ASMA, Celis JP, Froyen L (2003) Microstructure and interface characteristics of B_4C , SiC and Al_2O_3 reinforced Al matrix composites: a comparative study. *J Mater Process Technol* 142:738–743
- Chen Z (2005) Chemical thermodynamics of refractories. Metallurgical Industrial Publishing, Beijing, p 565
- Luo ZP (2006) Crystallography of SiC/Mg Al_4C_3 /Al interfaces in pre-oxidized SiC reinforced Al/SiC composite. *Acta Mater* 54(1):47–58
- Xiong Bowen, Yan Qingsong, Baiping Lu, Cai Changchun (2011) Effects of SiC volume fraction and aluminum particulate size on interfacial reactions in SiC nano-particulate reinforced aluminum matrix composites. *J Alloys Compd* 509:1187–1191
- Tomesanyi L, Varga K, Bartik I, Horanyi H, Maleczki E (1989) Electrochemical study of the pitting corrosion of aluminium and its alloys—II. Study of the interaction of chloride ions with a passive film on aluminium and initiation of pitting corrosion. *Electrochim Acta* 34(6):855–859

15. Anaee RA (2009) Effect of molybdate anions on corrosion behavior of SS 304 in 0.1 M NaCl solution. *Eng Technol J* 27(16):2931–2945
16. Anaee RA (2013) Galvanic corrosion of dental alloys in artificial saliva containing citric acid. *Eng Technol J* 31, Part A(12): 2299–2310
17. Hamilta O, Fernando M, Clarice T, Jesualdo L, Isolda C (2005) Corrosion performance of Al-Si-Cu hypereutectic alloys in a synthetic condensed automotive solution. *Mat Res* 8(2):155–159
18. Traldi SM, Costa I, Rossi JL (2001) Corrosion of spray formed Al-Si-Cu alloys in ethanol automobile fuel. *Key Eng Mater* 189–191:352–357
19. Anaee RA (2013) Sodium silicate and phosphate as corrosion inhibitors for mild steel in simulated cooling water system. *Arab J Sci Eng* 38(12):1–12
20. Anaee RA (2016) Behavior of Ti/HA in saliva at different temperatures as restorative materials. *J Bio Tribocorros*. doi:[10.1007/s40735-016-0036-1](https://doi.org/10.1007/s40735-016-0036-1)
21. Liu ZS, Huang GS, Gua MY (2006) Effect of hydrolysis of AlN particulates on the corrosion behavior of Al/AlNp composites. *Mater Chem Phys* 99:75–79
22. Nunes PCR, Ramanathan LV (1995) Corrosion behavior of alumina–aluminium and silicon carbide–aluminium metal–matrix composites. *Corrosion* 51:610–617